JOURNAL OF MECHANICS OF CONTINUA AND MATHEMATICAL SCIENCES
www.journalimcms.org

ISSN (Online): 2454 -7190, Vol.-20, No.-7, July (2025) pp 42-61 ISSN (Print) 0973-8975

THERMOPHORESIS AND BROWNIAN MOTION EFFECTS ON HEAT AND MASS TRANSFER IN MIXED CONVECTIVE MHD HYBRID NANOFLUID FLOW PAST AN INCLINED MAGNETIC STRETCHING SHEET WITH CHEMICAL REACTION AND HEAT SOURCE

David Kumar Parisa[1], K. Bhagya Swetha Latha[2], M. Gnaneswara Reddy[3]

[1]Research Scholar, Department of Mathematics, Acharya Nagarjuna University, Guntur, Andhra Pradesh, India-523001.

[2]Department of Mathematics, Vignan's Lara Institute of Technology and Science, Vadlamudi, Andhra Pradesh, India-522510.

[3]Department of Mathematics, Acharya Nagarjuna University Andhra Pradesh, India-523001.

Email: [1]davidkumarparisa862@gmail.com, [2]kswethalatha@gmail.com, [3]mgrmaths@gmail.com

Corresponding Author: **David Kumar Parisa**

https://doi.org/10.26782/jmcms.2025.07.00003

(Received: April 02, 2025; Revised: June 21, 2025; Accepted: July 04, 2025)

Abstract

This study investigates the influence of thermophoresis, Brownian motion, and inclined magnetic fields on magnetohydrodynamic (MHD) mixed convective flow of a chemically reacting hybrid nanofluid over an inclined magnetic stretching sheet. The hybrid nanofluid comprises copper (Cu) and aluminum oxide (Al_2O_3) nanoparticles suspended in blood, serving as the base fluid. A heat source and first-order chemical reaction are incorporated into the model to analyze their combined impact on velocity, temperature, and concentration profiles. The governing system of highly nonlinear partial differential equations (PDEs) is transformed into a set of ordinary differential equations (ODEs) using similarity transformations. These equations are numerically solved using the fourth-order Runge-Kutta method coupled with the shooting technique, implemented in MATLAB. Graphical results illustrate the effects of key dimensionless parameters such as magnetic field strength, thermophoretic and Brownian motion parameters, chemical reaction rate, and heat source on flow characteristics. The numerical results show excellent agreement with previously published studies, validating the accuracy of the methodology. The findings have potential applications in biomedical engineering, targeted drug delivery, and thermal management systems.

Keywords: Brownian motion, Chemical reaction, Heat source, Hybrid Nanofluid, Inclined magnetic field, Thermophoresis.

I. Introduction

Nanofluids, created by dispersing nanoscale particles into base fluids, have attracted significant attention due to their improved thermal properties and heat transfer performance. A further advancement in this field is the development of hybrid nanofluids, which combine two or more different nanoparticles in a single base fluid. These offer synergistic thermal behavior and enhanced heat transfer characteristics, outperforming conventional and mono-nanofluids [VII, XXVII].

Applications of hybrid nanofluids span a wide range of engineering systems, including plate heat exchangers, where the nanoparticle mixture ratio directly influences thermal performance [III]. In more complex scenarios, such as flows involving chemically reactive systems, magnetic fields, or porous media, hybrid nanofluids provide optimized thermal and mass transport behaviors. These are crucial in sectors like biomedical heat management, cooling of micro-electromechanical systems (MEMS), and industrial heat exchangers [XIX]. More recently, attention has shifted towards hybrid nanofluids, which integrate three different nanoparticles, unlocking superior control over viscosity, conductivity, and entropy generation. Such fluids have demonstrated promising results in configurations like stretching surfaces under electromagnetic effects, where thermal dissipation and entropy optimization are essential [VIII]. Studies also show that including Hall current, morphological effects, and non-Newtonian rheology further extends their usefulness in MHD flows between plates or channels [XXI]. Additionally, hybrid nanofluids have been effectively modeled in simulations involving magnetic fields, activation energy, and slender stretching geometries, suggesting potential in areas such as nanoelectronics cooling, magnetically targeted drug delivery, and thermal protection systems [I, VI, XV].

Magnetohydrodynamics (MHD) is a fascinating domain within fluid mechanics that deals with the motion of electrically conducting fluids under the influence of electromagnetic fields. One of the critical aspects of MHD is the Lorentz force, which acts perpendicular to both the magnetic field and the direction of fluid flow. On flat surfaces, this interaction is particularly significant, as it can lead to a retardation effect that slows down the fluid. This decelerative force can, however, be exploited effectively in certain processes to control and regulate fluid velocity, especially in industrial or energy systems. Despite its importance, the experimental validation of MHD phenomena remains limited, primarily due to challenges in replicating such environments under controlled laboratory conditions. Interestingly, MHD effects also manifest naturally, such as in the liquid core of the Earth, where magnetic fields influence geophysical flows. One of the key advantages of MHD is that it enables propulsion without moving mechanical parts, making it highly suitable for applications like nuclear reactors and other systems where mechanical wear must be minimized. For instance, Sreedevi et al. [XXVI] examined MHD flow involving carbon nanotubes over a conical surface under free convection. Reddy et al. [XXII] investigated the characteristics of MHD flow over a rotating disk embedded in a porous medium to better understand flow behavior under varied physical conditions.

Ramana et al. [XX] explored MHD effects in nanofluid flow using the Cattaneo–Christov thermal flux model, which accounts for finite speed of heat propagation. Further, Hazarika et al. [IX] demonstrated enhanced thermal performance by integrating different nanoparticles (Ag, Cu, and Fe_3O_4) into hybrid nanofluids subjected to MHD flows over flat surfaces. In another recent study, Sabu et al. [XXIII] examined the influence of nanoparticle shapes and MHD conditions on the flow of alumina–water hybrid nanofluids within a rotating system under convective boundary conditions, highlighting the critical interplay between magnetic fields, particle morphology, and boundary heat transfer.

Chemical reactions are ubiquitous in both natural and industrial processes, occurring at rates that range from extremely slow to rapid. Common examples include combustion of fuels, metal corrosion, glass and ceramic manufacturing, iron smelting, food processing, and even high-energy processes like nuclear fission and fusion. Due to their extensive practical relevance, researchers continue to investigate the dynamics and control of chemically reactive systems. For example, Irfan et al. [XI] examined the two-dimensional stagnation point flow of a chemically reacting Maxwell nanofluid over a stretching cylinder, highlighting how the mass transfer rate varies with the thermal Biot number under constructive and destructive chemical reaction scenarios. Khan et al. [XII] studied Maxwell nanofluid stagnation flow over a stretching surface while incorporating generalized diffusion effects. Similarly, Ibrahim et al. [X] applied a finite difference method to model chemically reactive Maxwell nanofluid flow over an elongated surface, considering velocity slip effects. Seyedi et al. [XXIV] conducted a numerical study on magnetohydrodynamic (MHD) Eyring–Powell squeezing flow in a channel under the influence of a chemical reaction.

Buongiorno [II] identified seven significant mechanisms that influence the convective transport of nanofluids, stemming from the movement of nanoparticles within the base fluid. Using scale analysis, these mechanisms include: nanoparticle size, inertia, particle agglomeration, Magnus effect, nanoparticle volume fraction, Brownian motion, and thermophoresis. Among these, Brownian motion and thermophoresis are found to be the most influential in enhancing heat transfer. Thermophoresis drives particles from high-temperature regions to low-temperature zones, working against the temperature gradient. In contrast, Brownian motion causes particles to migrate from regions of higher concentration to those of lower concentration. Nield and Kuznetsov [XVI] investigated the Cheng–Minkowycz problem for natural convection boundary-layer flow of a nanofluid in a porous medium. Subsequently, Kuznetsov and Nield [XV] extended the analysis by incorporating the effects of Brownian motion and thermophoresis in the natural convection boundary-layer flow over a vertical plate. Khan and Pop [XIII] analyzed the boundary-layer flow of a nanofluid past a stretching sheet, while Chamkha et al. [IV] focused on the mixed convection MHD flow of a nanofluid over a stretching permeable surface, considering the influences of Brownian motion and thermophoresis. Furthermore, Noghrehabadi et al. [XVII] examined the heat and mass transfer characteristics of non-Darcy natural convection nanofluid flow over a vertical cone embedded in porous media.

The novelty of this study lies in the comprehensive analysis of mixed convective MHD flow of a blood-based hybrid nanofluid containing copper (Cu) and aluminum oxide (Al_2O_3) nanoparticles past an inclined magnetic stretching sheet, under the combined influence of thermophoresis, Brownian motion, an inclined magnetic field, a heat source, and a chemical reaction. Unlike previous works that consider single nanofluids or simpler geometries, this research introduces a physiologically relevant base fluid (blood) and employs a hybrid nanoparticle combination, enhancing thermal conductivity and modeling accuracy for biomedical and thermal system applications. Furthermore, the incorporation of an exponentially stretching sheet provides a more realistic simulation of advanced manufacturing processes. The transformation of the governing PDEs into ODEs using similarity variables, followed by numerical integration through the Runge-Kutta fourth-order method with a shooting scheme, offers robust and validated results. This integrated approach presents new insights into the interactive roles of physical parameters on heat and mass transfer performance in hybrid nanofluid systems.

II. Mathematical Model

We investigate a two-dimensional, time-dependent, mixed convective boundary layer flow of a hybrid nanofluid composed of copper (Cu) and aluminum oxide (Al_2O_3) nanoparticles suspended in blood as the base fluid. The flow develops over an exponentially stretching, inclined, and permeable sheet in the presence of an inclined magnetic field, chemical reaction, internal heat source, thermophoresis, and Brownian motion effects. As depicted in Figure 1, the stretching surface is aligned at an angle α with the horizontal x-axis, while the ambient flow domain occupies the region $y \geq 0$ within a porous medium. The imposed magnetic field B is applied perpendicular to the surface but is inclined by angle α with the y-axis.

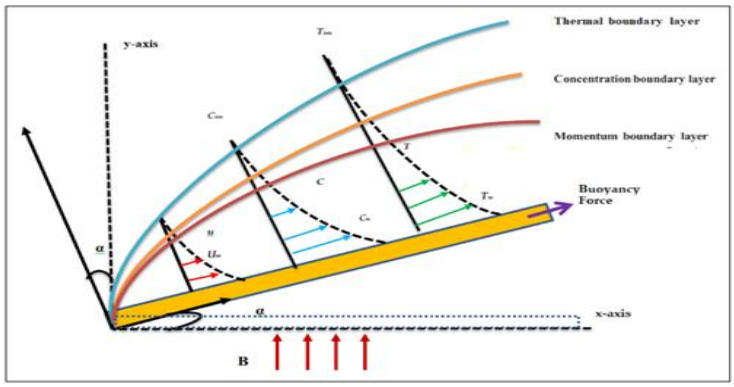

Fig. 1. Physical Configuration of the problem

The sheet stretches with a velocity $u_w(x)$, and due to suction or injection through the porous surface, the normal velocity component is taken as v=0. Thermal and solutal buoyancy forces are induced by temperature and concentration differences between the surface (Tw, Cw) and the ambient fluid (T_∞, C_∞). The interaction of thermophoresis and Brownian motion enhances nanoparticle movement, thereby affecting heat and mass transport. This leads to the development of distinct

momentum, thermal, and concentration boundary layers, governed by a system of nonlinear partial differential equations. These equations are reduced to ordinary differential equations via similarity transformations and solved numerically using the Runge-Kutta fourth-order method with a shooting technique.
The flow is governed by the equations [XIV]

Continuity Equation:

$$\frac{\partial u}{\partial x}+\frac{\partial v}{\partial y}=0 \tag{1}$$

Momentum Equation:

$$u\frac{\partial u}{\partial x}+v\frac{\partial u}{\partial y}=\frac{\mu_{hnf}}{\rho_{hnf}}\frac{\partial^2 u}{\partial y^2}-\frac{\sigma_{hnf}B_0^2}{\rho_{hnf}}Sin^2\gamma\, u+\frac{g(\rho\beta)_{hnf}}{\rho_{hnf}}(T-T_\infty)cos\alpha+\frac{g(\rho\beta)_{hnf}}{\rho_{hnf}}(C-C_\infty)cos\alpha \tag{2}$$

Energy Equation:

$$u\frac{\partial T}{\partial x}+v\frac{\partial T}{\partial y}=\frac{k_{hnf}}{\left(\rho C_p\right)_{hnf}}\frac{\partial^2 T}{\partial y^2}+\frac{Q_0}{\left(\rho C_p\right)_{hnf}}(T-T_\infty)+\tau_{hnf}\left(D_B\frac{\partial C}{\partial y}\frac{\partial T}{\partial y}+\frac{D_T}{T_\infty}\left(\frac{\partial T}{\partial y}\right)^2\right)-\frac{1}{\left(\rho C_p\right)_{hnf}}\frac{\partial q_r}{\partial y} \tag{3}$$

Concentration Equation:

$$u\frac{\partial C}{\partial x}+v\frac{\partial C}{\partial y}=D_B\frac{\partial^2 C}{\partial y^2}-K_1\left(Cw-C_\infty\right) \tag{4}$$

The boundary conditions that are appropriate for this flow are

$$u=u_w(x)\lambda+A_1\frac{\mu_{hnf}}{\rho_{hnf}}\frac{\partial u}{\partial y},\quad v=v_w, T=T_w(x)+B_1\frac{\partial T}{\partial y},\quad C=C_w(x)+C_1\frac{\partial c}{\partial y}\ \text{ at } y=0, \tag{5}$$

$$u\to 0,\quad v\to 0,\quad T\to T_\infty \qquad C\to C_\infty \qquad \text{as} \quad y\to\infty. \tag{6}$$

The velocity components in the x- and y-directions are denoted by u and v, respectively, with spatial coordinates x and y. Time is represented by t. The fluid temperature T, wall temperature $T_w(x)$, and ambient temperature T_∞ are considered. Species concentration within the fluid is C, with wall and ambient concentrations represented by $C_w(x)$ and C_∞, respectively. The hybrid nanofluid properties include density ρhnf, dynamic viscosity μhnf, and electrical conductivity σhnf. The magnetic field strength is denoted by B_0. Thermal expansion coefficient β, gravitational acceleration g, specific heat at constant pressure cp, and thermal conductivity of the hybrid nanofluid khn are also important parameters. Brownian diffusion and thermophoretic diffusion coefficients are represented by D_B and D_T. Volumetric heat

generation or absorption is given by Q_0, and radiative heat flux by q_r. The ratio of nanoparticle heat capacity to base fluid heat capacity is dimensionless and denoted by τhnf. The chemical reaction rate constant is K_1. Slip effects are captured by the velocity slip coefficient A_1, the thermal slip coefficient B_1, and the solutal slip coefficient C_1. The wall suction or injection velocity is v_w, and the velocity of the stretching sheet is $u_w(x)$.

The radiative heat flux qr can be expressed as

$$q_r = -\frac{4\sigma^*}{3k^*}\frac{\partial T^4}{\partial y} \tag{7}$$

where σ* is the Stefan–Boltzmann constant and k* is the absorption coefficient. Assuming that the temperature differences within the fluid are small, and following the approach of Patil et al. [XVIII], the term T^4 can be approximated by a Taylor series expansion about the ambient temperature T_∞.

We assume that the temperature variances inside the flow are such that the term T^4 can be represented as a linear function of temperature. This is accomplished by expanding T^4 in a Taylor series about a free stream temperature T_∞ as follows:

$$T^4 = T_\infty^4 + 4T_\infty^3(T - T_\infty) + 6T_\infty^2(T - T_\infty)^2 + \tag{8}$$

After neglecting higher-order terms in the above equation beyond the first-degree term in $(T - T_\infty)$, we get

$$T^4 \cong 4T_\infty^3 T - 3T_\infty^4 \tag{9}$$

Using (8) in (9) and then $\frac{\partial q_r}{\partial y}$ is

$$\frac{\partial q_r}{\partial y} = -\frac{16\sigma^* T_\infty^3}{3k^*}\frac{\partial^2 T}{\partial y^2} \tag{10}$$

The modified form of equation (3) can be written as

$$u\frac{\partial T}{\partial x} + v\frac{\partial T}{\partial y} = \frac{k_{hnf}}{(\rho C_p)_{hnf}}\frac{\partial^2 T}{\partial y^2} + \tau_{hnf}\left(D_B\frac{\partial C}{\partial y}\frac{\partial T}{\partial y} + \frac{D_T}{T_\infty}\left(\frac{\partial T}{\partial y}\right)^2\right) - \frac{1}{(\rho C_p)_{hnf}}\frac{16\sigma^* T_\infty^3}{3k^*}\frac{\partial^2 T}{\partial y^2} + \frac{Q_0}{(\rho C_p)_{hnf}}(T - T_\infty) \tag{11}$$

III. Similarity analysis

Introducing the following non-dimensional similarity variants for converting governing flow equations into a system of ordinary differential equations

$$\psi = e^{x/2L}\sqrt{2v_f Lc}f(\eta), u = \frac{\partial\psi}{\partial y}, v = -\frac{\partial\psi}{\partial x}, \eta = ye^{x/2L}\sqrt{\frac{c}{2v_f L}}, \theta(\eta) = \frac{T-T_\infty}{T_w-T_\infty}, \varphi(\eta) = \frac{C-C_\infty}{C_w-C_\infty} \quad (12)$$

The similarity transformation (12) is substituted into equations (1) to (11), and we have

$$\left(\frac{\left(\frac{\mu_{hnf}}{\mu_f}\right)}{\left(\frac{\rho_{hnf}}{\rho_f}\right)}\right)f''' + ff'' - 2f'^2 - \left(\frac{\left(\frac{\sigma_{hnf}}{\sigma_f}\right)}{\left(\frac{\rho_{hnf}}{\rho_f}\right)}\right)MSin^2\gamma\, f' + 2Gr\left(\frac{\left(\frac{(\rho\beta)_{hnf}}{\rho_f}\right)}{\left(\frac{\rho_{hnf}}{\rho_f}\right)}\right)\theta cos\alpha + 2Gc\left(\frac{\left(\frac{(\rho\beta)_{hnf}}{\rho_f}\right)}{\left(\frac{\rho_{hnf}}{\rho_f}\right)}\right)\Phi cos\alpha = 0 \quad (13)$$

$$\theta''\frac{(1+R\,\mathrm{Pr})}{\mathrm{Pr}} + \frac{\left(\frac{(\rho C_p)_{hnf}}{(\rho C_p)_f}\right)}{\left(\frac{k_{hnf}}{k_f}\right)}\left(f\theta' + N_b\theta'\phi' + N_t\theta'^2\right) + \frac{Q}{\left(\frac{k_{hnf}}{k_f}\right)}\theta = 0 \quad (14)$$

$$\varphi'' - Sc(4f\phi' - f\varphi) + 2Sc.Kr.\phi = 0 \quad (15)$$

$$f(0) = s, f(0) = \lambda + af'', f'(\infty) = 0, \theta(0) = 1 + B\theta'(0), \theta(\infty) = 0, \varphi(0) = 1 + C\varphi'(0), \varphi(\infty) = 0 \quad (16)$$

The dimensional quantities are

$$\begin{cases} M = \frac{\sigma B_0^2 e^{-\frac{x}{L}}}{c\rho_f}, Pr = \frac{\nu_f}{k_f} = \frac{(\nu\rho C_p)_f}{k_f}, \theta_w = \frac{T_w}{T_\infty}, Gr = \frac{g\beta_f T_0 L}{c^2}, Gc = \frac{g\beta_f C_0 L}{c^2}, S_c = \frac{\nu_f}{D_m} \\ K_r = \frac{K_1 L}{C}e^{-\frac{x}{L}}, Q = \frac{qL}{c(\rho C_p)_f}, R = \frac{4\sigma^* T_\infty^3}{k_f k^*}, N_b = \frac{\tau D_B(C_w - C_\infty)}{\nu}, N_t = \frac{\tau D_T(T_w - T_\infty)}{T_\infty \nu}. \end{cases} \quad (17)$$

Where A $= A_1\frac{\mu_{hnf}}{\rho_{hnf}}\, e^{\frac{x}{2L}}\sqrt{\frac{c}{2v_f L}}$ show the velocity slip factor, B = $B_1 e^{\frac{x}{2L}}\sqrt{\frac{c}{2v_f L}}$ denotes thermal slip factor, C = $C_1 e^{\frac{x}{2L}}\sqrt{\frac{c}{2v_f L}}$ expressed the concentration slip factor, and S = $-\nu_0/\sqrt{2v_f c/2L}$ the two main physical properties of relevance, the (Nux) and (Cf), are calculated as described as,

$$Cf_x = \frac{\mu_{hnf}}{\rho_{hnf}(u_w)^2}\left(\frac{\partial u}{\partial y}\right)_{y=0}, Nu_x = -\frac{(-2L)k_{hnf}}{k_f(T_w - T_\infty)}\left(\frac{\partial T}{\partial y}\right)_{y=0}, Sh_x = -\frac{(-2L)k_{hnf}}{k_f(C_w - C_\infty)}\left(\frac{\partial C}{\partial y}\right)_{y=0} \quad (18)$$

The Nusselt quantity, the Sherwood quantity, and the percentile of skin friction are all shown in their non-dimensional forms.

$$\mathrm{Re}_x^{1/2}\,C_f = \frac{\mu_{hnf}}{\mu_f} f''(0), \mathrm{Re}_x^{-\frac{1}{2}} C_f = -\frac{\mu_{hnf}}{\mu_f}\theta'(0), \mathrm{Re}_x^{-1/2}\,Sh_x = -\frac{k_{hnf}}{k_f}\varphi'(0) \quad (19)$$

The physical quantities used in the governing equations, along with their respective formulations for both nanofluid and hybrid nanofluid systems, are summarized in Table 1. These include properties such as dynamic viscosity, density, heat capacity, thermal conductivity, and electrical conductivity, all expressed in terms of nanoparticle volume fractions and base fluid properties. Additionally, the thermophysical properties of the materials involved, namely copper (Cu), aluminum oxide (Al_2O_3), and blood (used as the base fluid), are presented in Table 2 to support the computational analysis and enhance the accuracy of modeling efforts.

Table 1: Thermo-physical features for Nano fluids and hybrid Nano fluids.

Features	Nanofluid	Hybrid nanofluid
Dynamical viscidness (μ)	$\mu_{nf} = \mu_f(1-\varphi)^{-2.5}$	$\mu_{hnf} = \mu_f(1-\varphi_1)^{-2.5}(1-\varphi_2)^{-2.5}$
Density (ρ)	$\rho_{nf} = (1-\varphi)\rho_f - \varphi\rho_s$	$\rho_{hnf} = \left[(1-\varphi_2)\left\{(1-\varphi_1)\rho_f\right\} + \varphi_1\rho_{p_1}\right] - \varphi_2\rho_{p_2}$
Heat Capacity (ρc_p)	$(\rho c_p)_{nf} = (1-\varphi)(\rho c_p)_f - \varphi(\rho c_p)_s$	$(\rho c_p)_{hnf} = \left[(1-\varphi_2)\left\{(1-\varphi_1)(\rho c_p)_f + \varphi_1(\rho c_p)_{p_1}\right\}\right] - \varphi_2(\rho c_p)_{p_2}$
Thermal conductivity (k)	$\frac{k_{nf}}{k_f} = \left[\frac{(k_s+2k_f)-2\varphi(k_f-k_s)}{(k_s+2k_f)+\varphi(k_f-k_s)}\right]$	$\frac{k_{hnf}}{k_{gf}} = \left[\frac{(k_{p_2}+2k_{gf})-2\varphi_2(k_{gf}-k_{p_2})}{(k_{p_2}+2k_{gf})+\varphi_2(k_{gf}-k_{p_2})}\right]$ $\frac{k_{gf}}{k_f} = \left[\frac{(k_{p_1}+2k_f)-2\varphi_1(k_f-k_{p_1})}{(k_{p_1}+2k_f)+\varphi_1(k_f-k_{p_1})}\right]$
Electrical conductivity (σ)	$\frac{\sigma_{nf}}{\sigma_f} = \left[1+\frac{3\left(\frac{\sigma_s}{\sigma_f}-1\right)\varphi}{\left(\frac{\sigma_s}{\sigma_f}+2\right)-\left(\frac{\sigma_s}{\sigma_f}-1\right)\varphi}\right]$	$\frac{\sigma_{hnf}}{\sigma_f} = \left[1+\frac{3\left(\frac{\varphi_1\sigma_{p_1}+\varphi_2\sigma_{p_2}}{\sigma_f}-(\varphi_1+\varphi_2)\right)}{\left(\frac{\varphi_1\sigma_{p_1}+\varphi_2\sigma_{p_2}}{(\varphi_1+\varphi_2)\sigma_f}+2\right)-\left(\frac{\varphi_1\sigma_{p_1}+\varphi_2\sigma_{p_2}}{\sigma_f}-(\varphi_1+\varphi_2)\right)}\right]$

Table 2: Thermal physical properties.

Physical Properties	Blood	Al_2O_3	Cu
$\rho(\frac{kg}{m^3})$	1053	3970	8933
C_p(J/kgK)	3594	765	385
K(W/mk)	0.492	40	400

IV. Results and Discussion

This section presents a graphical analysis of the influence of various flow-controlling physical parameters on the thermo-physical behavior of hybrid nanofluid flow. The hybrid nanofluid under consideration consists of copper (Cu) and aluminum oxide (Al_2O_3) nanoparticles suspended in a base fluid of blood, which offers biocompatibility and enhanced thermal conductivity. The governing partial differential equations (PDEs), formulated based on the hybrid nanofluid model, are reduced to a system of ordinary differential equations (ODEs) using similarity transformations. The resulting similarity equations (Eqs. 13–15), along with the corresponding boundary conditions (Eq. 16), are numerically solved to investigate the effects of dimensionless physical parameters.

The key nondimensional parameters explored in this study include the magnetic parameter (M), the Thermophoresis parameter (Nt), the Brownian motion parameter (Nb), the Inclined magnetic field parameter (γ), Chemical reaction parameter (Kr). The principal aim of this analysis is to elucidate the effects of these parameters on the dimensionless velocity f′(η), temperature θ(η), and concentration ϕ(η) profiles of the hybrid nanofluid. The trends observed through the numerical simulation are depicted in the following graphical representations and discussed in detail to provide physical insight into the underlying transport mechanisms.

Figure 2–4 illustrates the effect of the thermal Grashof number Gr on velocity, temperature, and concentration profiles for Cu+Blood and Al_2O_3–Cu+Blood hybrid nanofluids. As Gr increases, the velocity profile rises due to enhanced buoyancy forces that accelerate the fluid motion. Conversely, the temperature and concentration profiles decrease with higher Gr, reflecting stronger thermal and solutal convection that thins the thermal and concentration boundary layers. The Al_2O_3–Cu+Blood nanofluid exhibits higher velocity, temperature, and concentration values compared to Cu+Blood, indicating that the inclusion of Al_2O_3 nanoparticles improves thermal and mass transport characteristics due to superior thermal conductivity and diffusivity.

Figures 5-7 present the effect of the solutal Grashof number Gc on the velocity, temperature, and concentration distributions for Cu+Blood and Al_2O_3–Cu+Blood hybrid nanofluids. As Gc increases, the velocity of the nanofluid rises due to stronger solutal buoyancy forces enhancing fluid motion. Simultaneously, both the temperature and concentration profiles decrease with increasing Gc, indicating more vigorous convective transport of heat and mass away from the surface. Additionally, the Al_2O_3–Cu+Blood hybrid nanofluid shows slightly higher velocity, temperature, and concentration levels than Cu+Blood, signifying improved transport characteristics resulting from the enhanced thermophysical properties of the hybrid composition.

Figures 8–10 show the influence of the magnetic parameter M on the velocity, temperature, and concentration distributions for Cu+Blood and Al_2O_3–Cu+Blood hybrid nanofluids. As M increases, the velocity decreases due to the Lorentz force, which resists fluid motion and suppresses momentum. Conversely, both temperature and concentration profiles rise with higher M, as the magnetic field generates additional resistive heating that enhances thermal and solutal energy within the boundary layer. The Al_2O_3–Cu+Blood hybrid nanofluid consistently exhibits stronger responses in all three profiles, highlighting its superior thermal conductivity and mass transport capacity compared to the mono-nanofluid (Cu+Blood).

Figures 11–13 display the effect of the magnetic field inclination angle γ on the velocity, temperature, and concentration profiles for both Cu+Blood and Al_2O_3–Cu+Blood hybrid nanofluids. As γ increases from π/8 to π/4, the velocity profile shows a moderate rise, indicating that a more inclined magnetic field reduces the effective Lorentz drag along the primary flow direction, allowing greater fluid motion. Additionally, both temperature and concentration profiles increase significantly with γ, suggesting enhanced thermal and solutal energy retention due to weakened magnetic resistance in the normal direction.

Figures 14 and 15 depict the impact of the Brownian motion parameter Nb on the temperature and concentration distributions for Cu+Blood and Al_2O_3–Cu+Blood hybrid nanofluids. As Nb increases, the temperature profile noticeably decreases, indicating that enhanced Brownian motion intensifies nanoparticle diffusion, leading to greater heat dispersion and thinner thermal boundary layers. In contrast, the concentration profile increases with Nb, as higher Brownian motion promotes the spread of nanoparticles, elevating solutal content throughout the fluid domain. The Al_2O_3–Cu+Blood hybrid nanofluid consistently shows lower temperature and higher concentration values compared to Cu+Blood, confirming the superior thermal diffusion and mass transport characteristics introduced by the hybrid composition.

Figures 16 and 17 illustrate the influence of the thermophoresis parameter Nt on the temperature and concentration profiles for Cu+Blood and Al_2O_3–Cu+Blood hybrid nanofluids. As Nt increases, the temperature profile declines significantly, indicating that thermophoretic forces drive nanoparticles from hotter to cooler regions, thereby enhancing thermal diffusion and thinning the thermal boundary layer. Conversely, the concentration profile rises with increasing Nt, since thermophoresis increases particle accumulation away from the wall, boosting concentration within the flow. The hybrid Al_2O_3–Cu+Blood nanofluid consistently demonstrates superior heat and mass transfer characteristics compared to Cu+Blood, due to its enhanced thermophysical properties.

Figures 18 and 19 display the effects of the thermal radiation parameter R and heat source parameter Q on the temperature profile for Cu+Blood and Al_2O_3–Cu+Blood hybrid nanofluids. As R increases, the temperature significantly decreases, indicating that stronger nonlinear thermal radiation enhances radiative heat loss, which cools the fluid and compresses the thermal boundary layer. On the other hand, increasing Q leads to a noticeable rise in temperature, as additional internal heat generation amplifies the thermal energy within the boundary layer. In both scenarios, the Al_2O_3–Cu+Blood hybrid nanofluid exhibits higher temperature values than Cu+Blood, reaffirming its superior thermal conductivity and improved heat absorption behavior under radiative and internal heating conditions.

Figure 20 shows the influence of the chemical reaction parameter Kr on the concentration profile for Cu+Blood and Al_2O_3–Cu+Blood hybrid nanofluids. As Kr increases, the concentration decreases markedly, indicating that stronger chemical reactions enhance the rate of species consumption, thereby reducing nanoparticle concentration throughout the boundary layer.

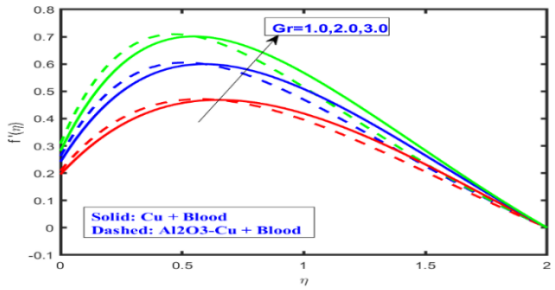

Fig. 2. Effect of Gr on Velocity

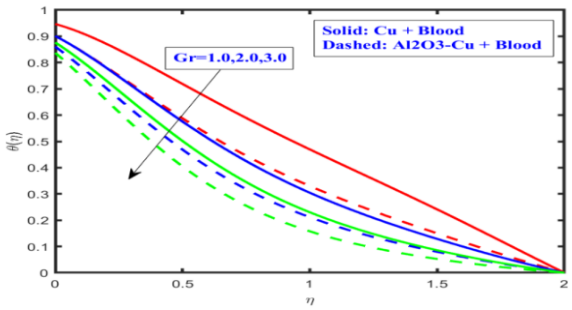

Fig. 3. Effect of Gr on Temperature

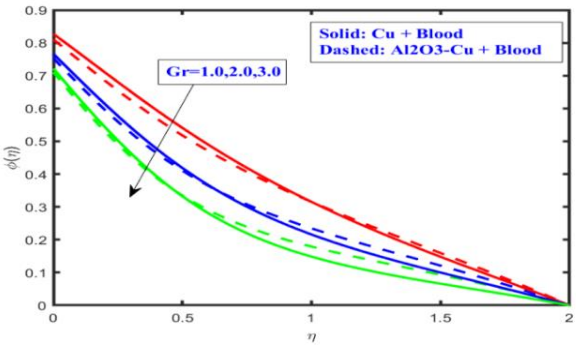

Fig. 4. Effect of Gr on Concentration

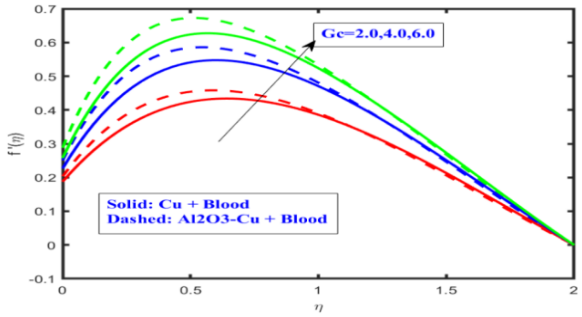

Fig. 5. Effect of Gc on Velocity

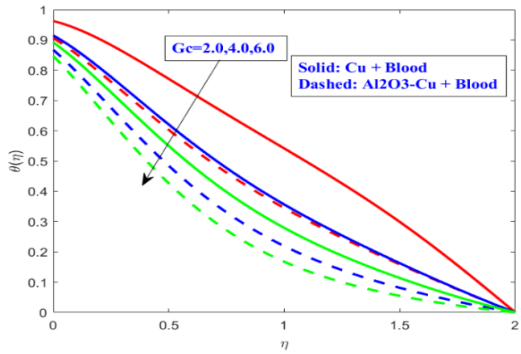

Fig. 6. Effect of Gc on Temperature

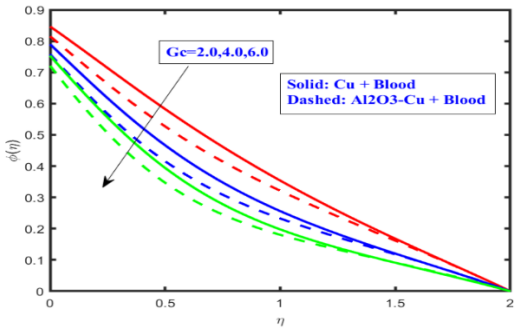

Fig. 7. Effect of Gc on Concentration

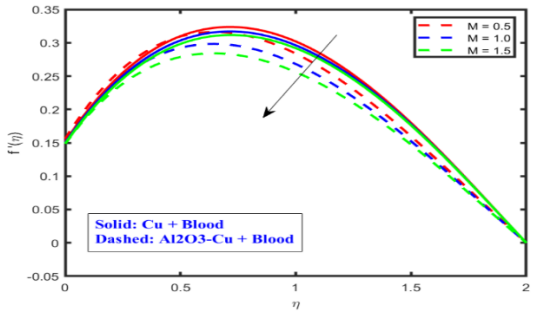

Fig. 8. Effect of M on Velocity

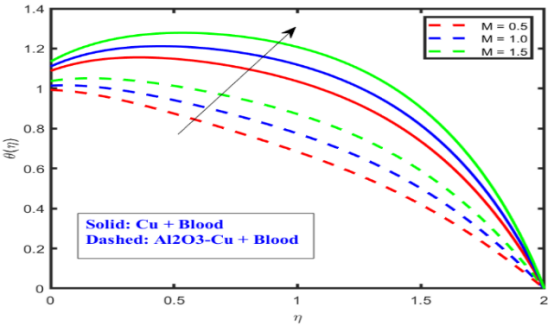

Fig. 9: Effect of M on Temperature

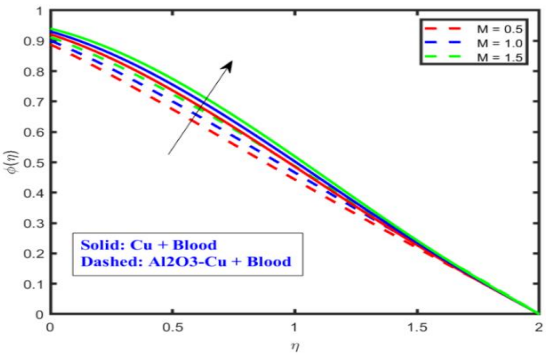

Fig. 10. Effect of M on Concentration

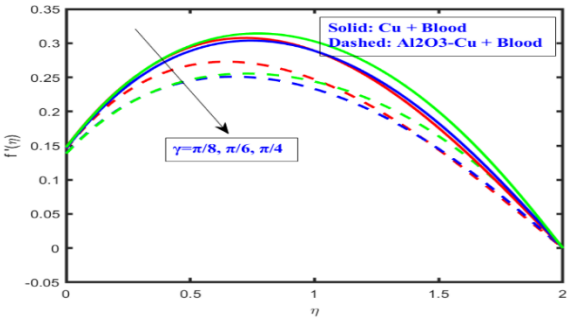

Fig. 11. Effect of γ on Velocity

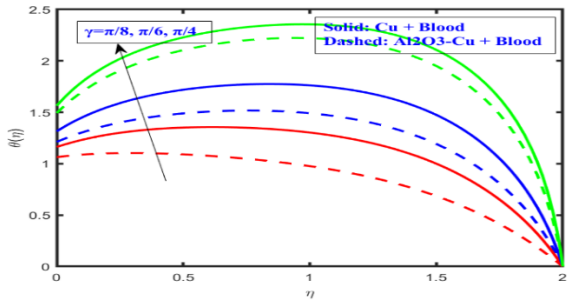

Fig. 12. Effect of γ on Temperature

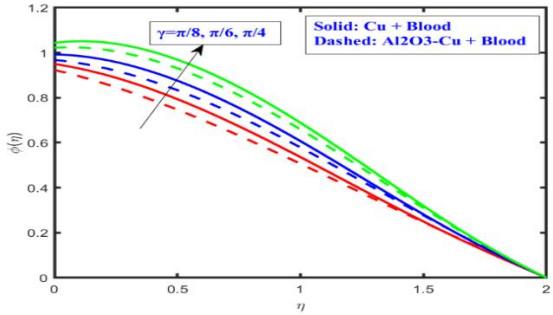

Fig. 13. Effect of γ on Concentration

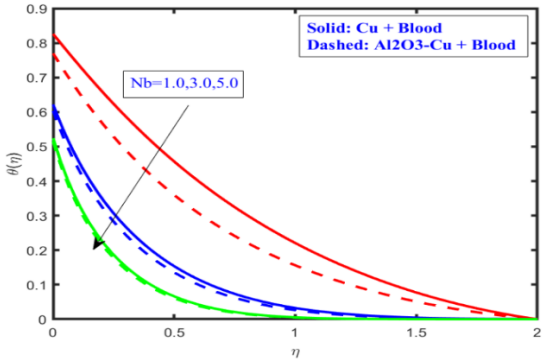

Fig. 14. Effect of Nb on Temperature

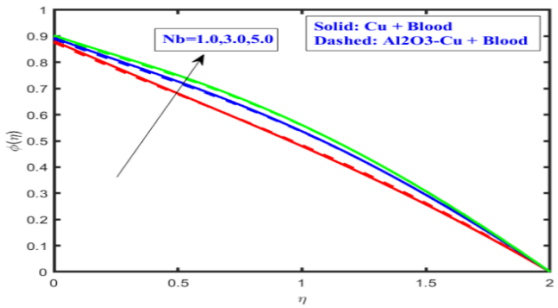

Fig. 15. Effect of Nb on Concentration

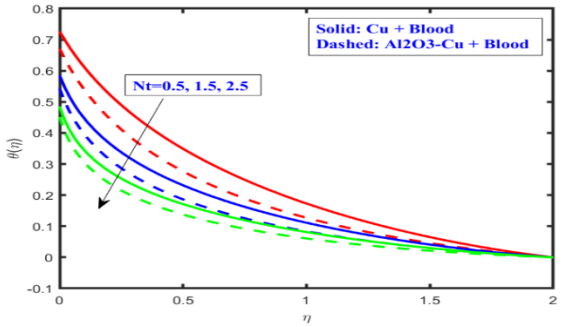

Fig. 16. Effect of Nt on Temperature

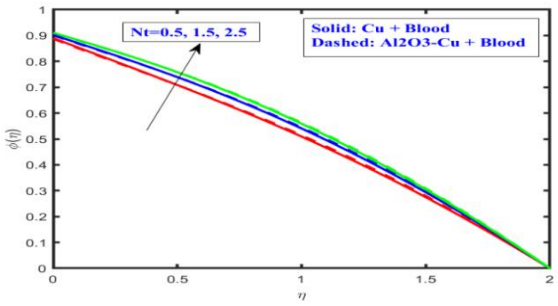

Fig. 17. Effect of Nt on Concentration

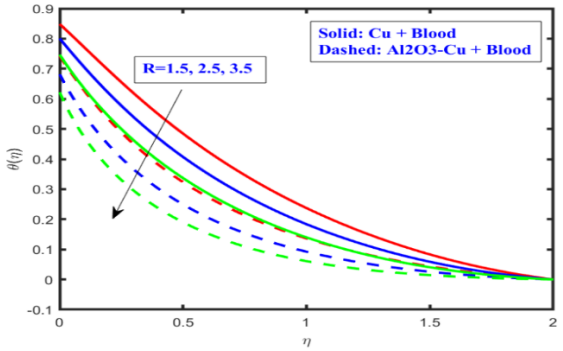

Fig. 18. Effect of R on Temperature

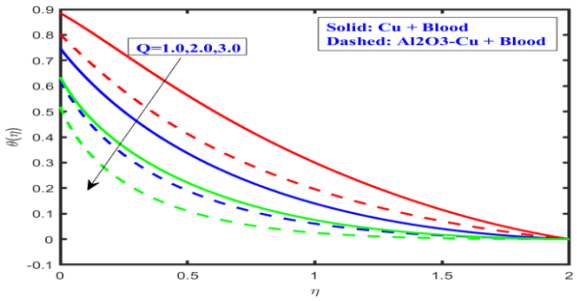

Fig. 19. Effect of Q on Temperature

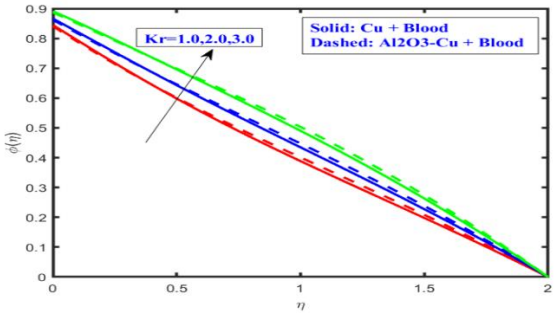

Fig. 20. Effect of Kr on Concentration

Table. 3: Variation in skin friction coefficient, Nusselt number, and Sherwood number under various physical parameters

M	Gr	Gc	γ	(Cf_x)	Nu_x	Sh_x
0.5	1	2	π/3	1.297841607	0.54551747	0.53677185
1	1	2	π/3	1.216849474	0.46074691	0.49209824
1.5	1	2	π/3	1.145000227	0.37055505	0.45036784
0.5	1	2	π/3	1.297841607	0.54551747	0.53677185
0.5	1	2	π/3	1.772634079	0.81354106	0.67780924
0.5	2	2	π/3	2.177942108	0.96806663	0.77605352
0.5	3	2	π/3	2.543431435	1.07889730	0.85591457
0.5	1	2	π/3	1.297841607	0.54551747	0.53677185
0.5	1	4	π/3	2.073532883	0.93402338	0.76367871
0.5	1	6	π/3	2.659435775	1.11005772	0.89953007
0.5	1	2	π/6	1.297848746	0.54587464	0.53678363
0.5	1	2	π/4	1.216883467	0.46073735	0.49274363
0.5	1	2	π/3	1.1457363345	0.370834643	0.45038262

An analysis of Table 3 reveals clear trends in the behavior of skin friction coefficient, Nusselt number, and Sherwood number in response to changes in key physical parameters. As the magnetic parameter M increases, all three quantities, skin friction, Nusselt number, and Sherwood number, decrease. This is due to the enhanced Lorentz force, which resists fluid motion and suppresses momentum, thermal, and mass transport. In contrast, an increase in the thermal Grashof number Gr leads to

higher values of skin friction, Nusselt number, and Sherwood number, as stronger buoyancy forces accelerate the fluid and enhance convective heat and mass transfer. Similarly, increasing the solutal Grashof number Gc improves all three transport quantities due to greater solutal buoyancy effects. However, when the inclination angle of the magnetic field γ increases, a slight decrease in skin friction, heat transfer, and mass transfer is observed.

Table 4 illustrates the effects of various physical parameters on the skin friction coefficient (Cf), Nusselt number (Nux), and Sherwood number (Shx). An increase in the Brownian motion parameter (Nb) enhances both Cf and Nux, indicating intensified momentum and heat transfer, while Shx decreases due to reduced concentration near the surface. Similarly, a rise in the thermophoresis parameter (Nt) leads to higher Cf and Nux but lowers Shx, as thermophoretic forces drive nanoparticles away from the heated surface. As the radiation parameter (R) increases, both Cf and Nux grow, reflecting enhanced thermal gradients, whereas Shx diminishes. Furthermore, increasing the chemical reaction parameter (Kr) results in elevated Cf and Nux, while Shx consistently declines, indicating that stronger reactions suppress mass diffusion. The heat source parameter (Q) remains constant across entries and thus shows no variation in this dataset.

Table 5 presents a comparative analysis of the present numerical results with those reported by Chandrakala and Srinivasa Rao [V] for the case when Nb=Nt=Q=0. The comparison reveals a close agreement between both sets of results, validating the accuracy and reliability of the present computations. Specifically, at the parameter value 0.0, the present solution yields 1.9367 and 0.9432, which are consistent with the literature values of 1.9367 and 0.9432, respectively. As the parameter increases to 0.5 and 1.0, the present results remain close to the reference values, confirming the robustness of the numerical scheme employed. This conformity underscores the credibility of the current model in capturing the physical behavior accurately.

Table. 4: Variation in skin friction coefficient, Nusselt number, and Sherwood number under various physical parameters

Nb	Nt	Q	R	Kr	(Cf_x)	Nu_x	Sh_x
1	0.1	1	1.5	1	1.4826202	2.4632398	0.34825503
2	0.1	1	1.5	1	1.5467234	2.8787574	0.30261391
3	0.1	1	1.5	1	1.5908630	3.1459414	0.26858463
1	0.2	1	1.5	1	1.5097169	2.6451298	0.32741310
1	0.3	1	1.5	1	1.5362107	2.8234526	0.30615263
1	0.1	1	1.5	1	1.4826202	2.4632398	0.34825503
1	0.1	2	1.5	1	1.4826202	2.4632398	0.34825503
1	0.1	3	1.5	1	1.4826202	2.4632398	0.34825503
1	0.1	1	3.5	1	1.5640474	2.95142362	0.29284127
1	0.1	1	5.5	1	1.6246838	3.29003464	0.24584903
1	0.1	1	1.5	1	1.4826202	2.46323989	0.34825503
1	0.1	1	1.5	2	1.50926252	2.49267252	0.30891624
1	0.1	1	1.5	3	1.56242326	2.56323989	0.28165242

Table 5: Comparison of numerical solution for $f'(\eta)$ with Nb=Nt=Q=0

η	Present values	Chandrakala and Srinivasa Rao [V]
0.0	1.936735678	0.943155
0.5	0.893893649	0.882399
1.0	0.887236356	0.813842

V. Conclusions

This study investigated the thermophysical behavior of a hybrid nanofluid composed of Cu and Al_2O_3 nanoparticles suspended in blood, subject to mixed convection and magnetohydrodynamic effects over a stretching surface. The governing nonlinear partial differential equations were transformed via similarity variables and solved numerically to analyze the effects of various physical parameters on velocity, temperature, and concentration distributions.

Increasing the thermal Grashof number (Gr) boosts velocity but reduces temperature and concentration due to intensified buoyancy-driven convection. A higher solutal Grashof number (Gc) increases velocity while decreasing temperature and concentration through stronger solutal buoyancy effects. The magnetic parameter (M) suppresses velocity due to the Lorentz force while enhancing temperature and concentration via resistive heating. An increase in magnetic field inclination angle (γ) raises velocity, temperature, and concentration by reducing the effective magnetic drag. Rising Brownian motion parameter (Nb) reduces temperature and increases concentration through enhanced nanoparticle diffusion. A greater thermophoresis parameter (Nt) lowers temperature and elevates concentration due to particle migration from hot to cold regions. Increasing thermal radiation parameter (R) decreases temperature by promoting radiative heat loss. Higher heat source parameter (Q) raises the temperature due to internal heat generation. The chemical reaction parameter (Kr) reduces concentration by accelerating species consumption.

VI. Limitations, Applications, and Future Scope

The present study provides important insights into the natural convection characteristics of nanofluids using a two-phase numerical simulation approach. However, several simplifying assumptions have been made that define the scope and applicability of the current model. Notably, the fluid is assumed to be Newtonian. In many biomedical and industrial applications, fluids may exhibit non-Newtonian behavior such as shear-thinning, viscoplasticity, or elastic effects, which can significantly influence flow and heat transfer patterns. Ignoring such effects limits the model's applicability in scenarios where fluid rheology plays a crucial role.

Additionally, in practical biomedical systems such as drug delivery or targeted thermal therapy, these factors can have a substantial impact. The model also employs static thermal and solutal boundary conditions, whereas real-world systems often involve time-dependent or spatially varying boundary inputs due to pulsatile flow or dynamic environmental influences.

Despite these limitations, the findings of this work have direct relevance to many practical engineering and biomedical applications. In the field of thermal management, the results may guide the design and optimization of heat exchangers, microchannel systems, and high-performance electronic cooling devices. In biomedical engineering, the simulation framework can be adapted for analysis of temperature control during hyperthermia treatments or the transport of nanoparticles in therapeutic applications. The work also offers useful insights for energy systems that employ nanofluids, such as solar thermal collectors and compact nuclear cooling technologies.

Looking ahead, several directions are proposed to expand and improve the current study. Future models could incorporate non-Newtonian fluid behavior to better simulate complex fluids in biological and industrial systems. Three-dimensional geometries and irregular domain modeling could further improve the physical realism of simulations, especially in biomedical contexts. Time-dependent analyses, such as pulsatile or transient flows, would provide a deeper understanding of unsteady convection effects. Furthermore, multi-physics coupling such as magnetohydrodynamics, heat generation, or electric field effects could broaden the applicability of the model in MEMS/NEMS and other emerging technologies.

Conflict of Interest:

There was no relevant conflict of interest regarding this paper.

References

I. Algehyne, E. A., Alrihieli, H. F., Bilal, M., Saeed, A., & Weera, W. (2022). Numerical approach toward ternary hybrid nanofluid flow using variable diffusion and non-Fourier's concept. *ACS Omega*, *7*(30), 29380–29390. 10.1021/acsomega.2c04309

II. Buongiorno, J. (2006). Convective transport in nanofluids. Journal of Heat Transfer, 128(3), 240–250. 10.1115/1.2150834

III. Bhattad, A., Sarkar, J., & Ghosh, P. (2020). Heat transfer characteristics of plate heat exchanger using hybrid nanofluids: Effect of nanoparticle mixture ratio. *Heat and Mass Transfer, 56*(9), 2457–2472. 10.1007/s00231-020-02864-z

IV. Chamkha, A. J., Aly, A. M., & Al-Mudhaf, H. (2011). Mixed convection flow of a nanofluid over a permeable stretching sheet in the presence of a magnetic field. International Journal of Microscale and Nanoscale Thermal and Fluid Transport Phenomena, 2(1), 51–72.

V. Chandrakala, P., Srinivasa Rao, V. (2024). Effect of Heat and Mass Transfer over Mixed Convective Hybrid Nanofluids past an Exponentially Stretching Sheet, CFD Letters 16, Issue 3, 125-140.

VI. Eid, M. R., & Nafe, M. A. (2022). Thermal conductivity variation and heat generation effects on magneto-hybrid nanofluid flow in a porous medium with slip condition. *Waves in Random and Complex Media, 32*(6), 1103–1127. 10.1080/17455030.2022.2032491

VII. Elsebaee, F. A. A., Bilal, M., Mahmoud, S. R., Balubaid, M., Shuaib, M., Asamoah, J. K. K., & Ali, A. (2023). Motile micro-organism based trihybrid nanofluid flow with an application of magnetic effect across a slender stretching sheet: Numerical approach. *AIP Advances, 13*(3), 035237. 10.1063/5.0139487

VIII. Guedri, K., Khan, A., Gul, T., Mukhtar, S., Alghamdi, W., Yassen, M. F., & Tag Eldin, E. (2022). Thermally dissipative flow and entropy analysis for electromagnetic trihybrid nanofluid flow past a stretching surface. *ACS Omega, 7*(41), 33432–33442. 10.1021/acsomega.2c03834

IX. Hazarika, S., Ahmed, S., & Chamkha, A. J. (2021). Numerical simulation of MHD hybrid nanofluid flow over a stretching surface: Influence of nanoparticle type and volume fraction. Mathematics and Computers in Simulation, 182, 819–832. 10.1016/j.matcom.2020.10.026

X. Ibrahim, W., & Negera, M. (2020). MHD slip flow of upper-convected Maxwell nanofluid over a stretching sheet with chemical reaction. *Journal of the Egyptian Mathematical Society, 28*, 1–28.

XI. Irfan, M., Khan, M., & Khan, W. A. (2020). Heat sink/source and chemical reaction in stagnation point flow of Maxwell nanofluid. *Applied Physics A, 126*(1), 1–8.

XII. Khan, M., Malik, M. Y., Salahuddin, T., et al. (2019). Generalized diffusion effects on Maxwell nanofluid stagnation point flow over a stretchable sheet with slip conditions and chemical reaction. *Journal of the Brazilian Society of Mechanical Sciences and Engineering, 41*(1), 1–9.

XIII. Khan, W. A., & Pop, I. (2010). Boundary-layer flow of a nanofluid past a stretching sheet. International Journal of Heat and Mass Transfer, 53(11–12), 2477–2483. 10.1016/j.ijheatmasstransfer.2010.01.032

XIV. Khan, A. S., Xu, H.-Y., & Khan, W. (2021). Magnetohydrodynamic Hybrid Nanofluid Flow Past an Exponentially Stretching Sheet with Slip Conditions. Mathematics, 9(24), 3291. 10.3390/math9243291

XV. Kuznetsov, A. V., & Nield, D. A. (2010). Natural convective boundary-layer flow of a nanofluid past a vertical plate. International Journal of Thermal Sciences, 49(2), 243–247. 10.1016/j.ijthermalsci.2009.07.015

XVI. Nield, D. A., & Kuznetsov, A. V. (2009). The Cheng–Minkowycz problem for natural convective boundary layer flow in a porous medium saturated by a nanofluid. International Journal of Heat and Mass Transfer, 52(25–26), 5792–5795. 10.1016/j.ijheatmasstransfer.2009.07.024

XVII. Noghrehabadi, A., Behseresht, A., Ghalambaz, M., & Behseresht, J. (2013). Heat and mass transfer of non-Darcy natural convection nanofluid flow over a vertical cone embedded in porous media. Journal of Thermophysics and Heat Transfer, 27(2), 334–342. 10.2514/1.T4086

XVIII. Patil, V.S., Patil A.B., Ganesh S, et al. (2021). Unsteady MHD flow of a nano Powell-Eyring fluid near stagnation point past a convectively heated stretching sheet in the existence of chemical reaction with thermal radiation. Materials Today: Proceedings, 44: 3767–3776.

XIX. Raizah, Z., Khan, A., Gul, T., Saeed, A., Bonyah, E., & Galal, A. M. (2023). Coupled Dufour and Soret effects on hybrid nanofluid flow through gyrating channel subject to chemically reactive Arrhenius activation energy. *Journal of Nanomaterials, 2023*, Article 6721294. 10.1155/2023/6721294

XX. Ramana, K. V., Reddy, G. R., Reddy, M. C., & Chamkha, A. J. (2021). Cattaneo–Christov model for MHD nanofluid flow past a stretching surface with thermal relaxation and viscous dissipation. Journal of Thermal Analysis and Calorimetry, 147, 2749–2761. 10.1007/s10973-020-09661-3

XXI. Rauf, A., Faisal, N. A., & Shah, T. B. (2022). Hall current and morphological effects on MHD micropolar non-Newtonian tri-hybrid nanofluid flow between two parallel surfaces. *Scientific Reports, 12*, 16608. 10.1038/s41598-022-20877-6

XXII. Reddy, P. S., Sreedevi, P., & Chamkha, A. J. (2017). Magnetohydrodynamic flow and heat transfer of nanofluids over a rotating disk embedded in porous media. Powder Technology, 307, 46–55. 10.1016/j.powtec.2016.11.013

XXIII. Sabu, A. S., Reddy, P. S., Sreedevi, P., & Chamkha, A. J. (2021). Effect of nanoparticle shape on MHD hybrid nanofluid flow in a rotating system with convective boundary conditions. International Communications in Heat and Mass Transfer, 129, 105711. 10.1016/j.icheatmasstransfer.2021.105711

XXIV. Seyedi, S. H., Saray, B. N., & Chamkha, A. J. (2020). Heat and mass transfer investigation of MHD Eyring–Powell flow in a stretching channel with chemical reactions. *Physica A: Statistical Mechanics and its Applications, 544*, 124109.

XXV. Shahzad, F., Jamshed, W., Eid, M. R., Ibrahim, R. W., Aslam, F., Isa, S. S. P. M., & Guedri, K. (2023). The effect of pressure gradient on MHD flow of a tri-hybrid Newtonian nanofluid in a circular channel. *Journal of Magnetism and Magnetic Materials, 568*, 170320. 10.1016/j.jmmm.2022.170320

XXVI. Sreedevi, P., Reddy, P. S., & Chamkha, A. J. (2018). Magnetohydrodynamic boundary-layer flow of nanofluids over a cone with free convection. International Journal of Mechanical Sciences, 135, 646. 10.1016/j.ijmecsci.2017.12.019

XXVII. Zhang, I., L., Bhatti, M. M., Michaelides, E. E., Marin, M., & Ellahi, R. (2022). Hybrid nanofluid flow towards an elastic surface with tantalum and nickel nanoparticles, under the influence of an induced magnetic field. *European Physical Journal Special Topics, 231*(1), 1–13. 10.1140/epjs/s11734-021-00293-7